Available online at www.sciencedirect.com
ScienceDirect
International Journal of Multiphase Flow 33 (2007) 833–848
International Journal of Multiphase Flow
www.elsevier.com/locate/ijmulflow

Efficient calculation of the history force at finite Reynolds numbers

A.J. Dorgan, E. Loth *

Department of Aerospace Engineering, University of Illinois at Urbana-Champaign, 306 Talbot Laboratory, 104 South Wright Street, Urbana, IL 61801-2935, USA

Received 21 June 2005; received in revised form 25 February 2007

Abstract

Well-acknowledged problems associated with modeling the history force in large, many-particle simulations are related to the need to store and integrate over the entire lifetime of the particle. To address this concern, a computationally efficient method for calculating the history force (the "window model") was developed based on the assumption of weak changes in acceleration in the recent relevant history of the particle. This assumption leads to the design of a model with a truncated integration interval which requires storage of and integration over a much shorter period of the particle's history compared to other history force models. The truncation of the integration window can yield more than an order of magnitude savings in CPU time. In a related study, the two empirical coefficients of the Mei & Adrian history force kernel have been optimized (based on comparison with experimental data for falling particles) to give improved predictions of the data. Both the new history force kernel and the window model have been investigated for a large range of experimental data yielding, to the authors' knowledge, the most extensive comparison yet conducted. For falling particles, the new history force kernel shows good predictions for particle Reynolds numbers ranging from 9 to 853 and density ratios from 1.17 to 9.32. Good predictions were also obtained using the window model when changes in particle relative acceleration over the window period were modest. For particles under forced oscillating in a quiescent fluid, the history kernel was generally reasonable but did not predict the peak forces well in all cases. This may be explained by noting that the assumption of a t^{-2} long-time dependence for the finite Reynolds number history force kernel may become invalid during rapid deceleration and wake ingestion (which can lead to exponential or t^{-1} behavior). However, the finite Reynolds number kernel gives better predictions in all cases than those made using the Basset history force. The window model was only reasonable for the oscillating particle cases when the changes in the relative particle acceleration over the integration window were small.

Keywords: History force; Window model; Basset force; Lagrangian particle tracking

* Corresponding author. Tel.: +1 217 244 5581; fax: +1 217 244 0720.
E-mail address: loth@uiuc.edu (E. Loth).

0301-9322/$ - see front matter © 2007 Elsevier Ltd. All rights reserved.
doi:10.1016/j.ijmultiphaseflow.2007.02.005

1. Introduction

1.1. Lagrangian particle momentum equation

To numerically model a multiphase flow, it is often important to use separate formulations for the different phases. The present research is concerned with the hydrodynamic forces acting on an isolated, non-spinning, spherical particle in a continuous-phase flow of spatially-uniform velocity. Particles treated in a Lagrangian framework with a point-force method update their centroid-averaged properties (position, velocity, etc.) along the path of an individual particle based on the state of the continuous-phase (Loth, 2000). The point-force treatment uses theoretical and/or empirical models to describe this force (rather than resolving the details of the flowfield over the particle surface), and thus allows simulation of a large number of particles. Herein, we focus on efficient and accurate description of the history force for various Reynolds numbers for which the jerk (time derivative of the acceleration) is weak.

In the limit of creeping flow conditions ($Re_p \ll 1$, where $Re_p = d_p V_{\mathrm{rel}}/\nu_f$), the particle equation of motion for a solid (or fully contaminated) sphere can be written in terms of the relative velocity of the particle $\mathbf{V}_{\mathrm{rel}} = \mathbf{V}_p - \mathbf{V}_{f@p}$, where subscript "$p$" denotes a particle quantity, subscript "f" denotes a continuous-phase quantity, and subscript "$f@p$" denotes continuous-phase conditions hypothetically extrapolated to the particle center. The equation of motion includes time derivatives of the form $\mathrm{d}/\mathrm{d}t$ taken along the particle path and derivatives of the form $\mathrm{D}/\mathrm{D}t$ taken along the continuous phase path. If Faxen forces and discontinuous velocity changes are neglected, the equation of motion (Maxey and Riley, 1983) can be written as

$$m_p \frac{\mathrm{d}\mathbf{V}_p}{\mathrm{d}t} = -\pi\mu_f d_p \mathbf{V}_{\mathrm{rel}} + m_p g + \rho_f \Omega_p \left(\frac{\mathrm{D}\mathbf{V}_{f@p}}{\mathrm{D}t} - \mathbf{g}\right) + C_{\mathrm{M}}\rho_f \Omega_p \left(\frac{\mathrm{d}\mathbf{V}_{f@p}}{\mathrm{d}t} - \frac{\mathrm{d}\mathbf{V}_p}{\mathrm{d}t}\right) - 3\pi\mu_f d_p \int_{-\infty}^{t} K_{\mathrm{Basset}}(t-\tau)\frac{\mathrm{d}\mathbf{V}_{\mathrm{rel}}}{\mathrm{d}\tau}\mathrm{d}\tau \tag{1}$$

In this expression, m is mass, $\mathbf{g}$ is the gravity vector, d is diameter, ρ is density, μ_f is molecular viscosity, and Ω is volume ($= \frac{\pi}{6} d_p^3$ for a sphere). The left-hand-side of Eq. (1) is the inertial force assuming constant particle mass. On the right-hand-side, the "point-forces" include, from left to right, the quasi-steady drag force, the particle body (gravitational) force, the stress gradient force (due to fluid acceleration and the hydrostatic pressure gradient), the added (or virtual) inertial mass force where the added mass coefficient (C_{M}) is 1/2, and the history force which accounts for unsteady drag effects due to the temporal development of the particle boundary layer and wake. For the creeping flow limit, the history force kernel is

$$K_{\mathrm{Basset}}(t-\tau) = \left[\frac{4\pi(t-\tau)\nu_f}{d_p^2}\right]^{-1/2} \tag{2}$$

where $\mu_f = \nu_f \rho_f$. Eqs. (1) and (2) combine to give the well-known the Basset–Boussinesq–Oseen equation (Crowe et al., 1998).

Since inertial effects and drag often dominate particle dynamics, researchers typically define a particle response time based on these forces as $\tau_p \equiv (\rho_p + \rho_f C_{\mathrm{M}}) d_p^2/18\mu_f$. If the magnitude of τ_p compared to a relevant fluid time scale (i.e. the Stokes number) is large we would expect drag to negligibly affect the particle trajectory. Conversely, the particle motion can be dominated by drag effects when the Stokes number is small, with history forces becoming important for periods of high relative acceleration. The importance of the history force is also related to the particle density ratio, $\psi = \rho_p/\rho_f$, where, generally speaking, low density ratio particles ($\psi \ll 1$) and those of order unity ($\psi \sim 1$) can be significantly affected by the history force while high density ratio particles ($\psi \gg 1$) will be negligibly affected (Armenio and Fiorotto, 2001).

In this study, the appropriate form of the particle equation of motion at finite Reynolds numbers is considered. While the body force, inertial force, and fluid stress force are insensitive to Reynolds number (Druzhinin and Elghobashi, 1998), the quasi-steady and unsteady drag force as well as the added mass force require modification from the creeping flow expressions. The added mass force, as given in Eq. (1), incurs a subtle modification for inviscid conditions (Auton et al., 1988) such that the fluid acceleration term in the

added-mass force must be defined along the fluid-path ($D\mathbf{V}_{f@p}/Dt$). This form was found to be reasonable for a large range of Reynolds number by resolved-surface simulations (Mei et al., 1991; Kim et al., 1998) and experiments (Mei and Klausner, 1992; Bataille et al., 1991). Furthermore, the inviscid form effectively reverts to that in Eq. (1) at creeping flow conditions so that the Auton version may be generally employed (Maxey and Riley, 1983).

The quasi-steady drag term can be modified to account for finite Reynolds number effects by multiplying the creeping flow result by a "Stokesian correction factor", f. The empirical correlation given by White (1991) gives a reasonable representation of the spherical-particle steady drag for a wide range of Reynolds numbers

$$f = 1 + \frac{Re_p}{4(1+\sqrt{Re_p})} + \frac{Re_p}{60} \quad \text{for } Re_p < 2\times 10^5 \tag{3}$$

Based on the above, the finite Reynolds number equation of motion can expressed in terms of particle response time (τ_p), and density ratio as

$$\frac{d\mathbf{V}_p}{dt} = -\frac{1}{\tau_p} f \mathbf{V}_{\text{rel}} + \frac{1+C_M}{\psi + C_M}\frac{D\mathbf{V}_f}{Dt} + \frac{\psi - 1}{\psi + C_M}\mathbf{g} - \frac{1}{\tau_p}\int_{-\infty}^{t} K(t-\tau)\frac{d\mathbf{V}_{\text{rel}}}{d\tau}\,d\tau \tag{4}$$

where K is left as a general function to be discussed in the following section.

1.2. Particle history force at finite Reynolds numbers and long times

In general, the long-time behavior of the history force kernel for an unsteady flowfield with finite Re_p values is not fully understood. Mei and Adrian (1992) used results from resolved-surface simulations conducted by Mei et al. (1991) and an asymptotic analysis to investigate the history force at finite convective conditions for small amplitude (10%) fluctuations of the mean flow (no flow reversal). They determined that the limiting behavior yields a short-time period decay rate proportional to $t^{-1/2}$ (as given by the creeping flow expression, K_{Basset}) while the long-time decay rate is much faster and proportional to t^{-2}. They further suggested an interpolation between the short and long-time limits to obtain a model reasonable for the history force kernel for Re_p values up to 100 (see Fig. 3 of Mei and Adrian, 1992, and associated discussion) as

$$K((t-\tau,\tau),c_1,c_2) = \left\{ \left[\frac{4\pi(t-\tau)}{\tau_d}\right]^{1/2c_1} + \left[\frac{\pi(t-\tau)^2}{f_h \tau_d^2} Re_p^3\right]^{1/c_1} \right\}^{-c_1} \quad \text{with}$$
$$f_H = (0.75 + c_2 Re_p)^3 \tag{5}$$

In this form, the times are non-dimensionalized by the diffusive (viscous) time-scale $\tau_d = d_p^2/\nu_f$. The specific constants used for the Mei & Adrian kernel (K_{Mei}) were obtained by matching their oscillating flow simulations which yielded $c_1 = 2$ and $c_2 = 0.105$.

It was later shown that t^{-2} behavior was not universally valid. For example, Lovalenti and Brady (1993) observed exponential decay rates of the kernel for long-times while Mei (1994) found that the long-time decay rate for an impulsively started flow could be described as algebraic decay faster than t^{-2} or as a "slow exponential" decay. Lawrence and Mei (1995) show that the appropriate long-time decay rate for a particle falling from rest to terminal velocity is t^{-2}, but found different behavior for a particle suddenly coming to rest or undergoing flow reversal where the decay rate is t^{-1}. Similar findings were reported by Lovalenti and Brady (1995) who examined the history force analytically and noted that the transition from the short-time decay rate of $t^{-1/2}$ to a more rapid long-term decay depends on whether the particle was being accelerated or decelerated.

Kim et al. (1998) developed a more detailed semi-empirical formulation (including six constants determined by calibration with resolved-surface simulations) with the goal of increased robustness using a more detailed combination of the $t^{-1/2}$ and t^{-2} dependence. The Kim et al. model for weak accelerations is given by Eq. (5) where their values of the constants are $c_1 = 2.5$ and $c_2 = 0.126$ based on their own resolved-surface

simulations. As such, there is some disagreement on how best to model the transition from short-time behavior to long-time behavior with the effects of Reynolds number in terms of the values of c_1 and c_2. However, the form of Eq. (5) is deemed reasonable for simple flows so long as the particle does not ingest its own wake due to an abrupt stop, rapid deceleration, or direction reversal.

1.3. Objectives of current study

The motivation for this work is two-fold: (1) we seek improvements in accuracy of history force modeling using the form given in Eq. (5) based on detailed comparison with experiment and (2) we seek a computationally efficient way to compute the history force for finite Reynolds number particles. The first objective arose because there are different values of c_1 and c_2 available in the literature and because there has not been a comprehensive comparison with all available quantitative experiments in this matter. The second objective was motivated by the significant (and sometimes prohibitive) computational cost of calculating the history force integral for many particles (which includes the entire life time of the particle). The memory requirements needed to store the full history of particle information and the CPU requirements needed to compute the kernel at a large number integration points can become problematic for many multiphase flows. For example, storing the three-dimensional relative velocity for 100,000 particles (consistent with previous simulations by Dorgan and Loth, 2004) for 1000 time-steps using 4-byte real values would require 1.2 GB of memory.

To establish a more efficient method for computing the history force integral (that would reduce the required CPU hours and memory requirement), a "window model" was developed. This was inspired by the experiments of Mordant and Pinton (2000) who noted that the history force at finite Re_p was well represented by the creeping flow expression for short time periods (consistent with resolved-surface simulations of Chang and Maxey, 1994), but that the history force became negligible after a finite time interval. This is consistent with similar experiments by Moorman (1955) and the nature of Eq. (5). This suggests that the finite Re_p history force can be represented by the creeping flow history force "clipped" at some finite time which may be achieved by replacing the lower limit of integration with $t - t_{\text{window}}$, where t_{window} is obtained by assuming the relevant acceleration is approximately constant and by equating the integral with that which would have been obtained by Eq. (5).

2. Methodology

This section first discusses the optimization of the constants c_1 and c_2 (Eq. (5)) based on experimental data, particularly the falling particle data given by Moorman (1955). Herein, a "falling particle" is one released from rest and allowed to accelerate to terminal velocity under the influence of gravity. An efficient way for computing the new kernel (for any values of these constants) will be discussed in the remainder of the section. In all the simulations, a very fine temporal resolution of $0.001\tau_p$ was used to insure time-step independence since only single particles in simple flows were considered (though generally $0.1\tau_p$ is sufficient for accurate simulation of drag-dominated particles).

2.1. Calibration of c_1 and c_2 for falling particles

A number of the falling particle data sets given by Moorman (1955) were examined and compared to the predictions given by the Mei & Adrian and Kim et al. history force kernels. Three typical data sets (which have a density ratio of 3.69 and terminal Reynolds numbers ranging from 28.2 to 166) are shown in Fig. 1 along with predictions made using the various coefficient sets for the history force kernel of Eq. (5) as well as a prediction made using no history force. The experimental data correspond to, in order of increasing Reynolds number, Run #22, #21, #19 as given in Table 1. While the Mei & Adrian and approximate Kim et al. history kernels give much better predictions than the Basset force kernel, they tend to slightly over-predict the velocities (under-predict the history force) associated with the Moorman data. This minor deficiency can be generally improved for the Moorman data by using $c_1 = 2.5$ and $c_2 = 0.2$ (labeled "present kernel" in Fig. 1). These values were also found to be quite robust for the falling particle data of Mordant and Pinton (2000).

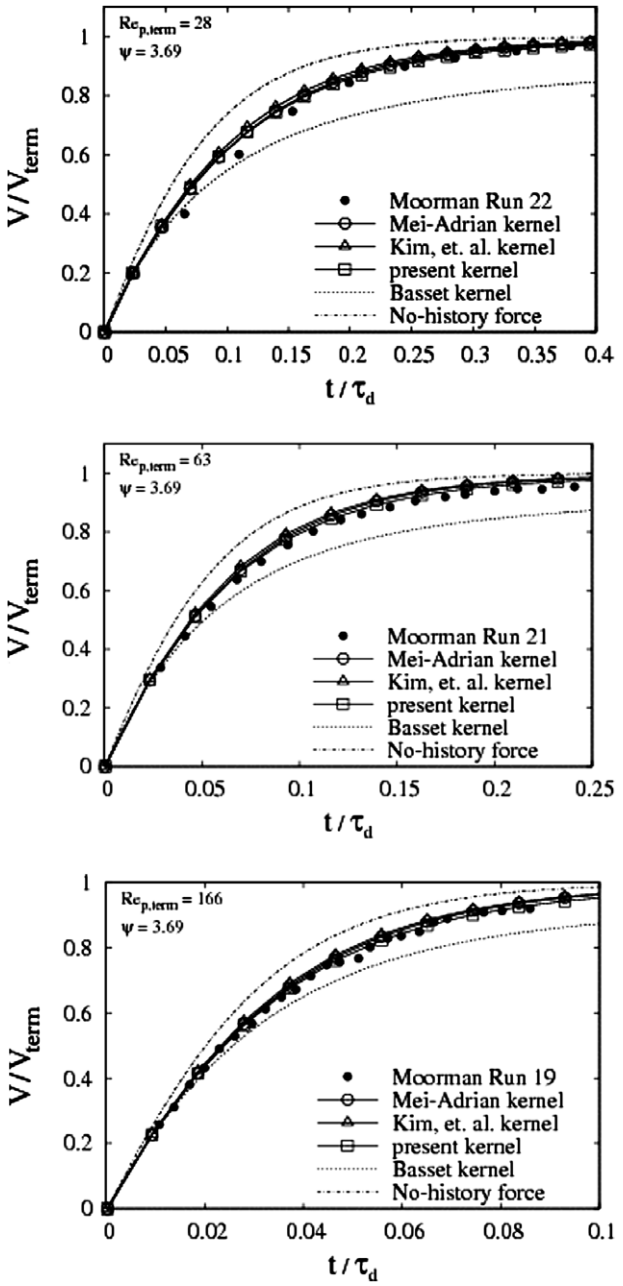

Fig. 1. Comparison of the various history force kernels with falling particle experiments of constant density ratio and various terminal Reynolds numbers.

2.2. Development of the window model

In general, evaluating the history force kernels discussed above requires integration over a temporal range of $\tau = -\infty$ to $\tau = t$ regardless of Reynolds number. The concept behind the window model is simple—we wish to prescribe a finite integration window such that the history force only requires integration over a temporal range of $\tau = t - t_{\text{window}}$ to $\tau = t$ which can be represented by the kernel K_{window},

Table 1
Experimental data sets considered in the present study

Run #	$Re_{p,term}$	ψ	$t_{window}/(\tau_p/f)$
Moorman			
9	55	9.32	0.11
10	31	9.15	0.10
11	15	9.15	0.09
12	9	9.15	0.10
17	600	3.51	1.16
18	301	3.51	0.71
19	166	3.69	0.46
21	63	3.69	0.28
22	28	3.69	0.22
26	45	2.47	0.35
27	29	2.47	0.31
28	15	2.47	0.30
32	853	1.65	2.85
33	319	1.22	1.71
34	231	1.41	1.24
35	136	1.72	0.77
36	48	1.27	0.60
37	15	1.17	0.53
M&P			
1	43	2.57	0.33
4	260	7.73	0.31
Odar			
9	11.5	0.911	1.16
18	30	0.911	2.13
29	6.5	1.77	1.85
38	17	1.77	2.80
50	20	0.589	1.03
56	36	0.589	1.59
65	30	0.442	1.04
68	39	0.442	1.27

(a) The Moorman (1955) experiments, (b) the Mordant and Pinton (2000) experiments, and (c) the Odar (1962) experiments.

$$K_{window}(t-\tau) = \begin{matrix} K_{Basset}, \\ 0 \end{matrix} \quad \text{for} \quad \begin{matrix} t - t_{window} < \tau < t, \\ \tau < t - t_{window}. \end{matrix} \tag{6}$$

If such a window can be specified, only the particle history for a time length of t_{window} would need to be stored and integrated for each particle.

The primary assumption for the window model is that the particle acceleration is constant (or nearly so) over the recent relevant time, i.e. the window duration. In this case, the history force can be correctly retained by equating the integral of the window kernel to that obtained for finite Reynolds number, i.e.

$$\int_{t-t_{window}}^{t} K_{window}((t-\tau),\tau)\,d\tau = \int_{-\infty}^{t} K((t-\tau),\tau)\,d\tau \tag{7}$$

The left integral can be evaluated analytically for long times since K_{window} is either zero or equal to K_{Basset}. Performing this integration leads to a dimensionless window function (β) given by

$$\beta = \frac{t_{window}}{\tau_d} = \pi\left[\int_{-\infty}^{t} K\,d\tau\right]^2 \tag{8}$$

Another option would have been to normalize the window time by the convective time-scale ($\tau_c = d/V_{rel}$) which is more important at high Re_p (whereas τ_d is more important at low Re_p). However, both time-scales

will be incorporated since we will take $\beta = f(K(Re_p))$ and since $Re_p = \tau_d/\tau_c$. For short-times (where $t < \beta\tau_d$), the lower limit of integration reverts to the creeping flow limit ($t = 0$) after which it is given by Eq. (8), i.e.

$$t - t_{\text{window}} \equiv \max(0, t - \beta\tau_d) \tag{9}$$

Therefore, the total integration time will initially grow but eventually reaches a point where only a portion of the particle history will be considered.

The function β can be obtained by integrating the kernel of Eq. (5) for a given Re_p and choice of c_1 and c_2. As shown in Fig. 2, the integrations of the Mei & Adrian, Kim *et al.*, and present history force kernels (shown as symbols) can be accurately represented by the following three curve fits (shown as lines):

$$\beta_{\text{M\&A}} = \left(\frac{0.632}{Re_p} + 0.087\right)^2 \tag{10a}$$

$$\beta_{\text{Kim}} = \left(\frac{0.502}{Re_p} + 0.074\right)^2 \tag{10b}$$

$$\beta_{\text{present}} = \left(\frac{0.502}{Re_p} + 0.123\right)^2 \tag{10c}$$

Note that the present dimensionless window function is more similar to the Kim et al. model at low Re_p but is closer to (yet greater than) the Mei & Adrian model at large Reynolds numbers.

As previously mentioned, the window model is only valid if the changes in acceleration over t_{window} are sufficiently small once the long-time behavior is realized. (Note that for short-times, changes in acceleration are modeled appropriately as the window model reverts to the Basset kernel for the case of $t_{\text{window}} > t$, Eq. (9).) As such, we define ε to be the ratio of the change in acceleration over the window to the change in acceleration over the particle's trajectory, i.e.

$$\varepsilon = \frac{J_{\text{window}} t_{\text{window}}}{J_{\text{tra}j}\tau_{\text{tra}j}} \tag{11}$$

where J is the derivative of acceleration (i.e. the "jerk") and $\tau_{\text{tra}j}$ is a time-scale relevant to the changes in relative velocity the particle will experience. For negligible changes in acceleration over the window period we require $\varepsilon \ll 1$. If we assume that the ratio of the two jerks is of order unity (which was verified for most of the particle falling cases) we can write

$$\varepsilon \approx \frac{t_{\text{window}}}{\tau_{\text{tra}j}} \tag{12}$$

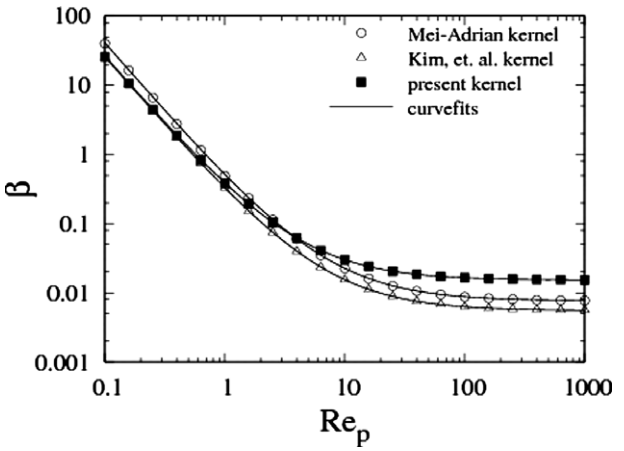

Fig. 2. The window model parameter for three history force kernels.

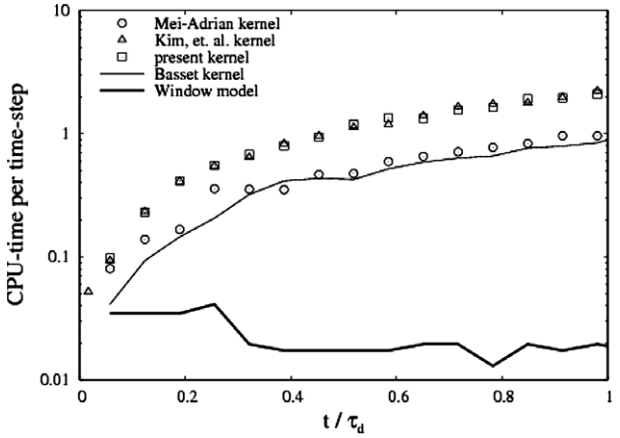

Fig. 3. Normalized CPU-time per time-step for the various history force expressions applied to Moorman Run 27.

For falling particle we will choose $\tau_{\mathrm{tra}j} = \tau_p/f$ and for oscillating particles we will choose $\tau_{\mathrm{tra}j} = \tau_f/2$, where τ_f is the period of the particle oscillation (for the relative velocity). In these cases, ε can be roughly approximated as

$$\varepsilon \approx \frac{18\beta}{\psi + C_{\mathrm{M}}} f \quad \text{falling particle} \tag{13a}$$

$$\varepsilon \approx 4\beta Re_{p,\mathrm{rms}} S \quad \text{oscillating particle} \tag{13b}$$

For the falling particle case, the Re_p used for β and f is based on terminal conditions for simplicity. For the oscillating particle case, $Re_{p,\mathrm{rms}}$ is based on $V_{\mathrm{rel,rms}}$ while S is the Strouhal number defined as

$$S = \frac{d_p}{2\tau_f V'_{\mathrm{rel,rms}}} \tag{14}$$

where $V'_{\mathrm{rel,rms}}$ is the root-mean-square (rms) of the relative velocity fluctuations about the mean. In the results section we will show that the above rough approximations to ε are a good indicator for the window model limits of applicability.

2.3. Computational expense

The key advantage of the window model compared to conventional history force expressions is its relatively small storage and its comparatively few number of required integration points; both of which result from a finite lower limit of integration. A quantitative comparison of the computational cost per time-step was performed for a falling particle simulation and the results are presented in Fig. 3. For this particular case, a savings of nearly two orders of magnitude is seen for integration times nearing one τ_d compared to the Basset and Mei & Adrian expressions. Thus, in cases where the window model formulation remains valid (i.e. sufficiently small ε) the savings in CPU-time for a many particle simulation is quite substantial. A minor but interesting point is that the Kim et al. and present kernels take approximately twice the CPU-time as compared to the Mei & Adrian kernel. This is due to the value of c_1 for these kernels (in both cases $c_1 = 2.5$) which leads to floating point exponentiation which much be done in software routines. This is in contrast to the Mei & Adrian kernel whose square operation involves only integer exponentiation (i.e. multiplication) and a square-root, both of which can be done at the hardware level at much greater speed.

3. Results

In this section we compare the predictions of the present kernel and the window model (using Eq. (10c)) with example experimental data. To assess the robustness and accuracy of the window model for the falling

particle data set of Moorman (1955), we first consider variation of particle Reynolds number (for a fixed density ratio) and secondly a variation of particle density ratio (for a fixed Reynolds number). The falling particle section is concluded by comparing both the window model and present kernel to data from Mordant and Pinton (2000). Similar comparisons will be made in the following sections for some cases of the oscillating particle data of Odar (1962). Table 1 summarizes the conditions for these cases and for the cases in Appendices A and B, which include all the other experimental cases for which sufficient quantitative data was available (some cases had too few data points or uncertainties in the initial conditions and so were not included). The predictions in Appendices support all the general statements made for the example cases discussed in the

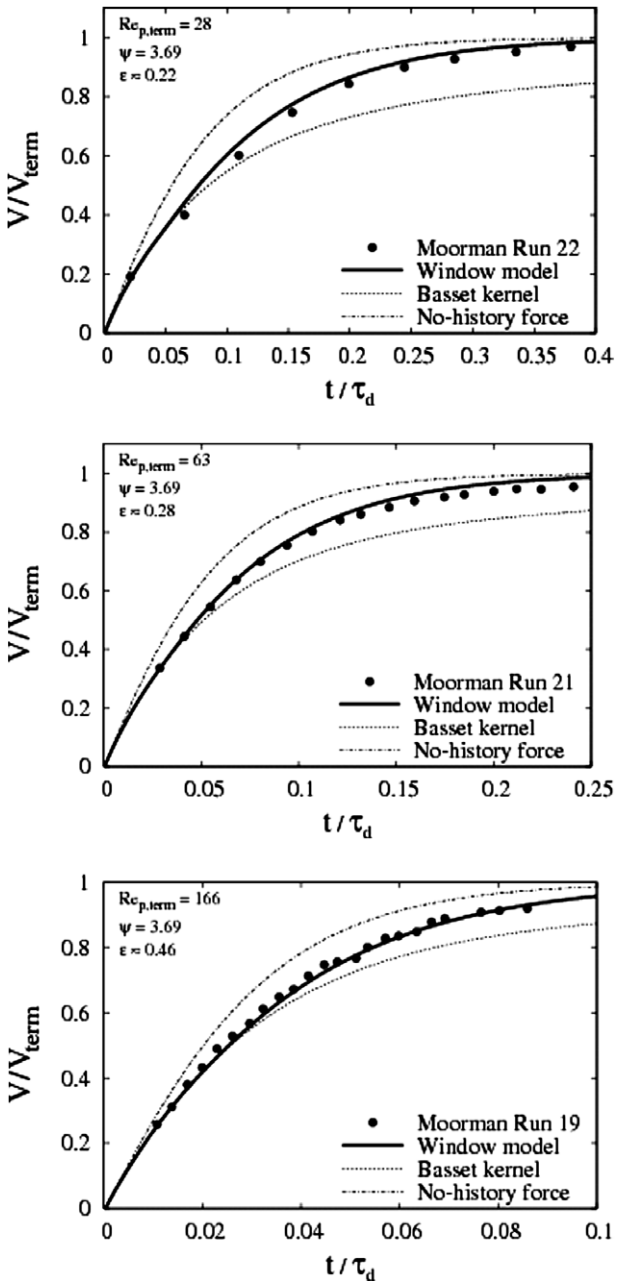

Fig. 4. Comparison of the window model with falling particle experiments of constant density ratio and various terminal Reynolds numbers.

results and are shown in order of increasing ε to illustrate deterioration of the model as that parameter increases.

The ability of the window model was first assessed by predicting the velocity of a particle with density ratio 3.69 and three different terminal Reynolds numbers (varying from 166 to 28.2). This is shown in Fig. 4 where the present model is compared to experimental data given by Moorman (1955), as well as predictions made using the Basset kernel and predictions without the history force. The model gives good agreement with

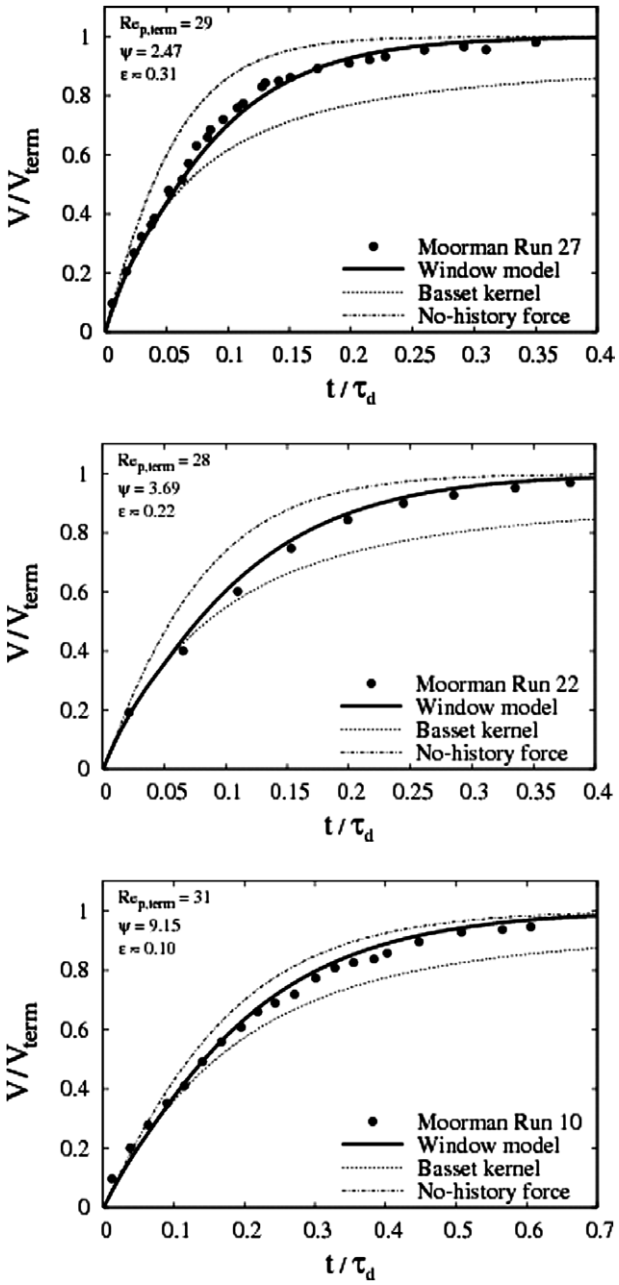

Fig. 5. Comparison of the window model with falling particle experiments with approximately constant terminal Reynolds number and varying density ratios.

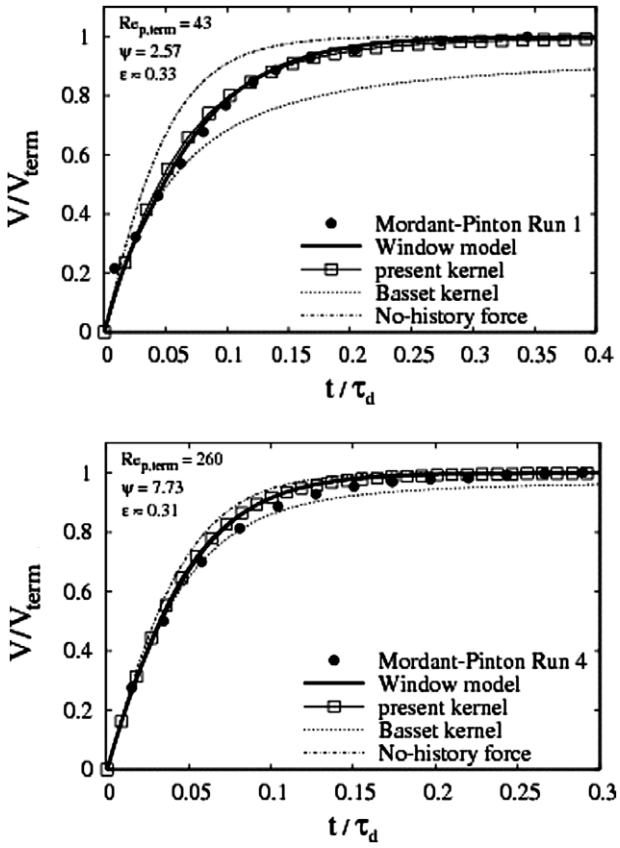

Fig. 6. The present model compared with experiments from Mordant and Pinton (2000).

the data and with the kernel predictions given in Fig. 1. Next, a variation in density ratio in the Moorman (1955) data is similarly compared in Fig. 5. The importance of the history force is seen to increase as density ratio decreases as the window model again performs well compared to the experimental data.

Two selected cases of the falling particle experiments of Mordant and Pinton (2000) are shown in Fig. 6. Both the window model and present kernel perform reasonably well for the case of $Re_{p,term}$ values of 43 and 260 given there is some experimental uncertainty (ca. 1–2%) in the velocity measurements. Notably, the window model gives the same result as the present kernel and both provide better predictions of the experimental data than that based on the Basset history force or no history force at all.

The oscillating particle experiments of Odar (1962) are considered to illustrate performance on a second flowfield. Odar forced a particle to oscillate in a vat of fluid and recorded the total hydrodynamic force observed during steady-state oscillation. Note that this experimental setup causes the particle to ingest is own wake as it reaches the end points of the oscillation. In Fig. 7, Odar's measured hydrodynamic surface force, F_{hydro}, (normalized by the quasi-steady drag based on the rms relative velocity) is compared with numerical predictions as a function of dimensionless time. Note that Fig. 7a and b have different Reynolds numbers but the same Strouhal number, while Fig. 7b and c have the different Strouhal numbers but the same Reynolds number. Finally, Fig. 7d is for the highest Strouhal number (1.77) considered by Odar. As discussed in Section 1.2, the long-time decay rate (t^{-2}) assumed by the kernel of the form given in Eq. (5) may not be appropriate, regardless of the values of c_1 and c_2. This is because the particle stops and reverses direction leading to wake ingesting which can alter the long-time decay rate to exponential or even t^{-1} if these events occur abruptly. However, the predictions made by the Mei & Adrian and present kernels are reasonable indicating this effect is generally not large for the present conditions (S or order unity or less), especially considering that

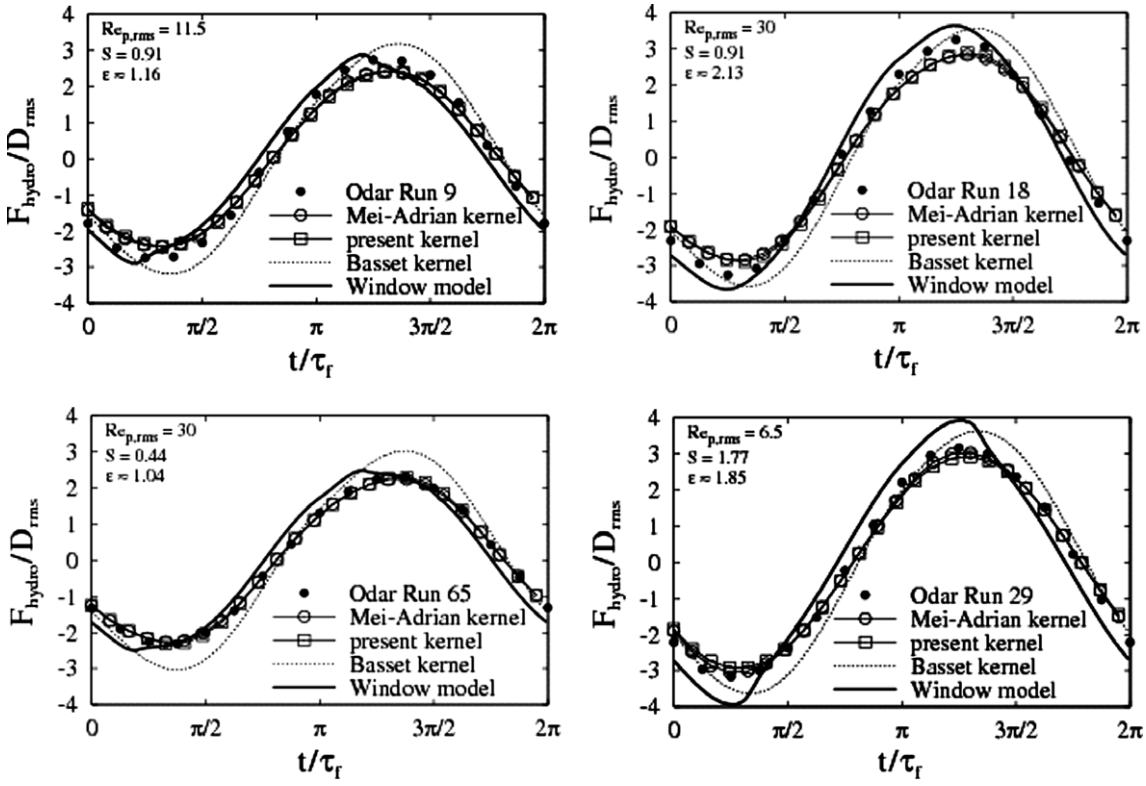

Fig. 7. Comparison of the present model with oscillating particle experiments of Odar (1962).

the unsteady drag shown here may be a small portion of the total drag. It is likely that the errant decay rate would become more evident for the higher Strouhal number cases ($S \gg 1$) where the reversal of relative velocity is more violent.

Fig. 7 also shows predictions made using the window model version of the present kernel. Here we note that the predictions are substantially different than those made by the present kernel and can even be worse than predictions made using the Basset kernel. Additionally, a non-physical change in slope is seen around the upper and lower peaks where the slope changes too quickly compared to the data. These problems are generally related to the range of applicability of the window model as discussed below.

The data shown in Figs. 4–6 and the cases in Appendices A and B indicate good agreement between the window model and experimental data until ε becomes somewhat greater than unity. This is qualitatively consistent with our expectations and illustrates the model's limitations. However, the simple definitions of ε employed herein involve quantities that are generally known a priori such that the applicability of the window model may be assessed prior to simulating a particle's trajectory. In the presence of turbulence this is less obvious but Dorgan and Loth (2004) give a model for estimating $V'_{\mathrm{rel,rms}}$ and $Re_{p,\mathrm{rms}}$ so that Eqs. (13b) and (14) can be estimated. However, turbulence introduces several other issues (e.g. non-rectilinear motion, spatial gradients of the flow, wide ranges of frequencies, etc.) that require further study.

4. Summary

The two coefficients of the history force kernel given by Mei and Adrian (1992) were optimized based on quantitative comparison with experimental data given by Moorman (1955). This included particle terminal

Reynolds numbers ranging from 9 to 853 and density ratios ranging from 1.17 to 9.32. Good agreement with the falling particle data of Mordant and Pinton (2000) was also obtained using these new coefficients.

A new and efficient method, the window model, was developed for computing the history force integral for finite Reynolds number particles and was based on the assumption of weak changes in acceleration within the window. The window model can be applied to any generic history force kernel and can result in orders of magnitude reduction in CPU-time compared to conventional history force calculations. The model was shown to perform well when predicting the behavior of falling particles provided ε was sufficiently small (e.g. less than unity).

For the oscillating particle experiments of Odar (1962), the history force kernels were not as accurate (though still reasonable) in cases where rapid wake ingestion occurred, i.e. $S > 1$. This is attributed to assumption of a t^{-2} long-time dependence which is invalid during rapid deceleration (when it can become exponential or t^{-1} behavior). More substantial errors were introduced when applying the window model to these conditions, since they were often associated with high changes in acceleration over the window period with ε greater than unity.

Acknowledgements

The authors would like to especially thank Drs. P. Lovalenti, R. Mei, and J.-F. Pinton for their valuable comments and suggestions.

Appendix A

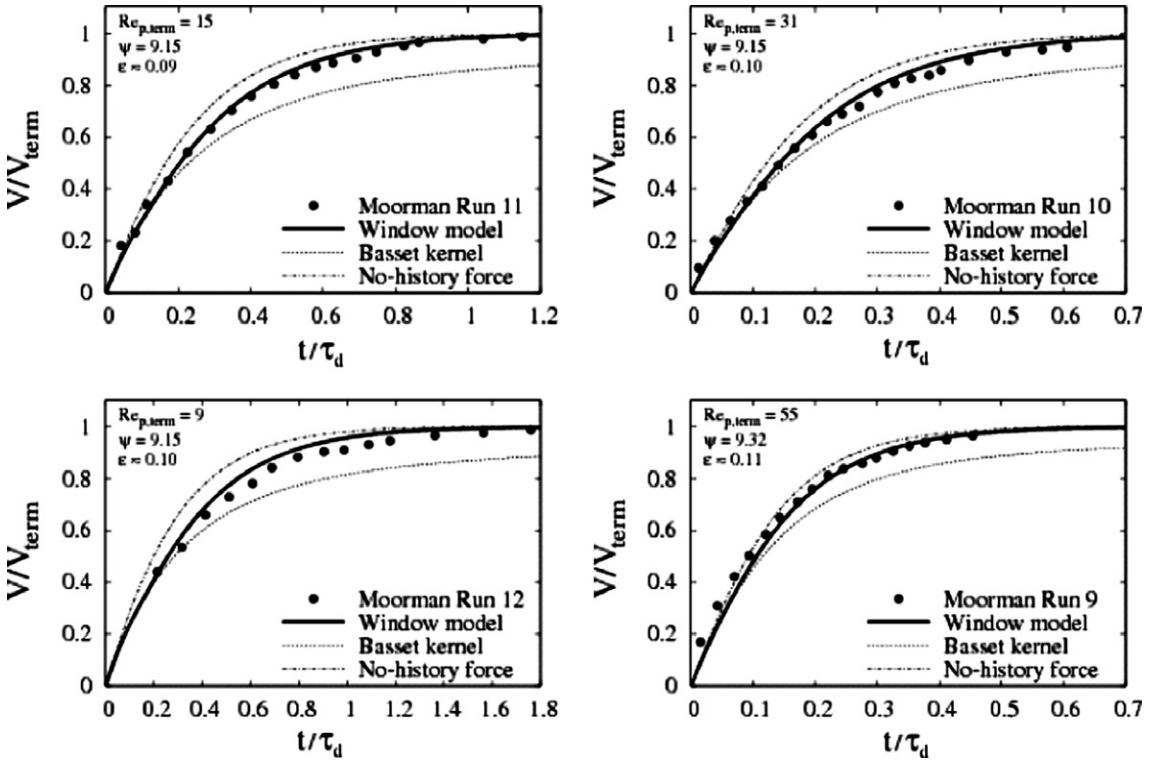

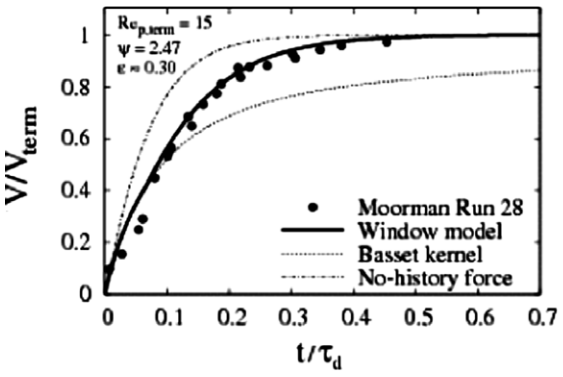
Re_p,term = 15
ψ = 2.47
ε ≈ 0.30
Moorman Run 28
Window model
Basset kernel
No-history force
V/V_term
t/τ_d

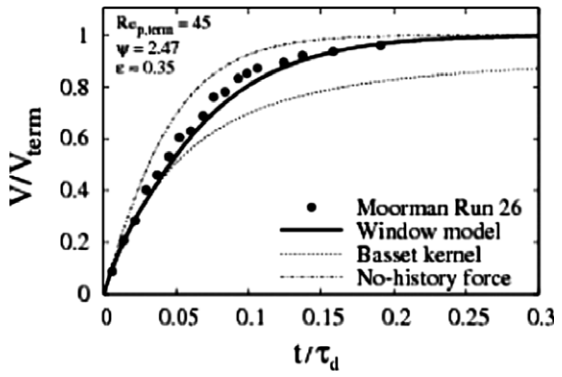
Re_p,term = 45
ψ = 2.47
ε ≈ 0.35
Moorman Run 26
Window model
Basset kernel
No-history force
V/V_term
t/τ_d

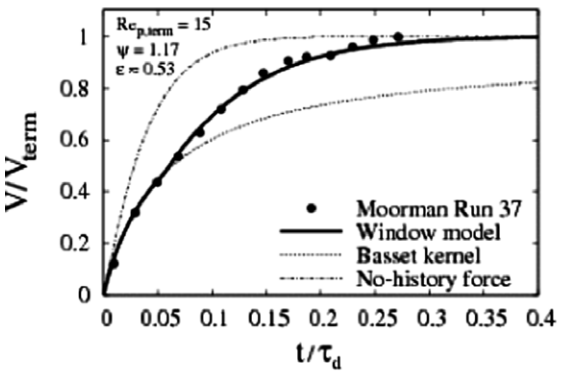
Re_p,term = 15
ψ = 1.17
ε ≈ 0.53
Moorman Run 37
Window model
Basset kernel
No-history force
V/V_term
t/τ_d

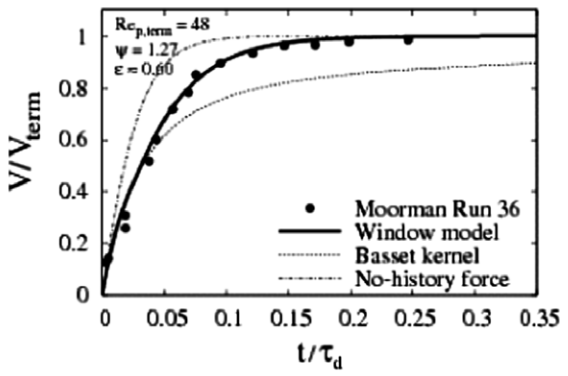
Re_p,term = 48
ψ = 1.27
ε ≈ 0.60
Moorman Run 36
Window model
Basset kernel
No-history force
V/V_term
t/τ_d

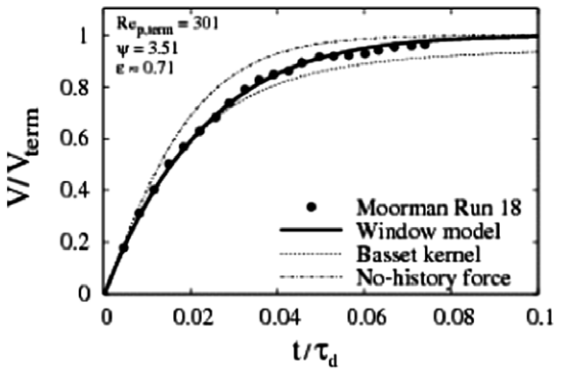
Re_p,term = 301
ψ = 3.51
ε ≈ 0.71
Moorman Run 18
Window model
Basset kernel
No-history force
V/V_term
t/τ_d

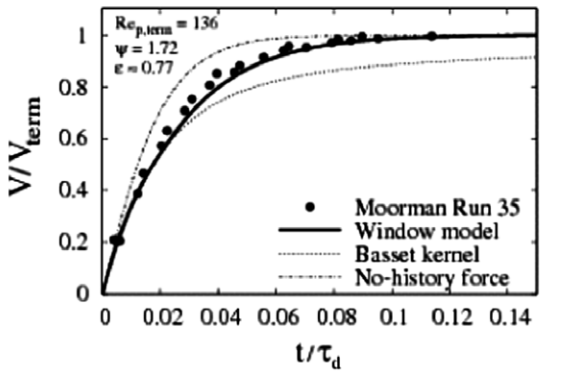
Re_p,term = 136
ψ = 1.72
ε ≈ 0.77
Moorman Run 35
Window model
Basset kernel
No-history force
V/V_term
t/τ_d

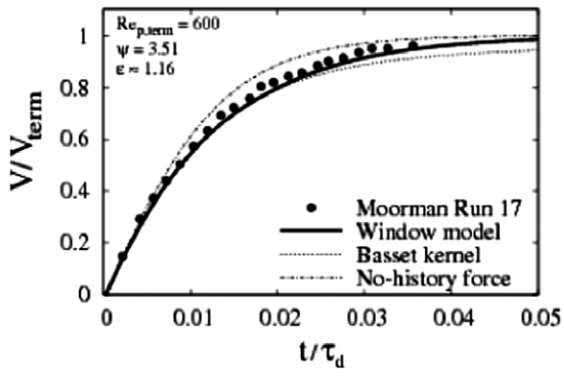
Re_p,term = 600
ψ = 3.51
ε ≈ 1.16
Moorman Run 17
Window model
Basset kernel
No-history force
V/V_term
t/τ_d

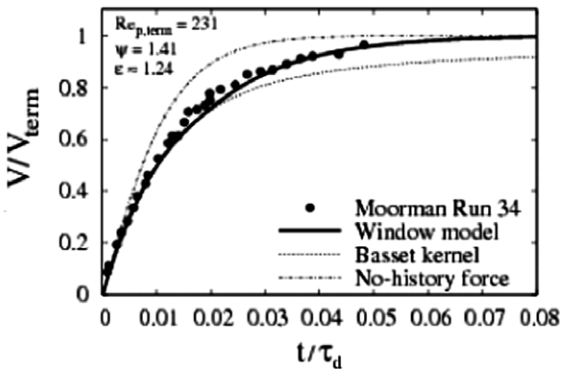
Re_p,term = 231
ψ = 1.41
ε ≈ 1.24
Moorman Run 34
Window model
Basset kernel
No-history force
V/V_term
t/τ_d

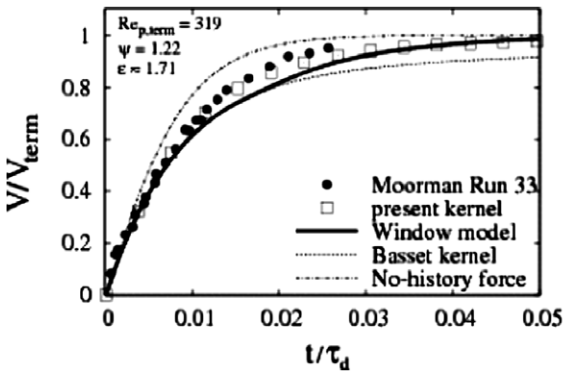

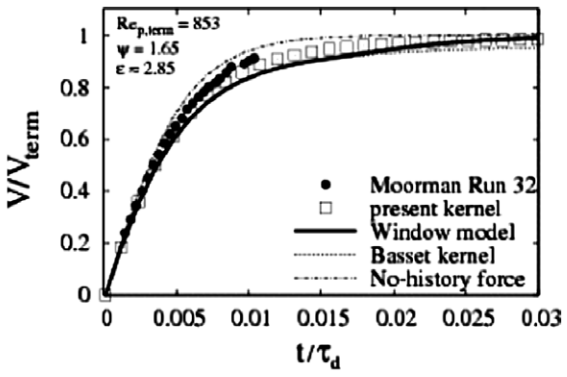

Appendix B

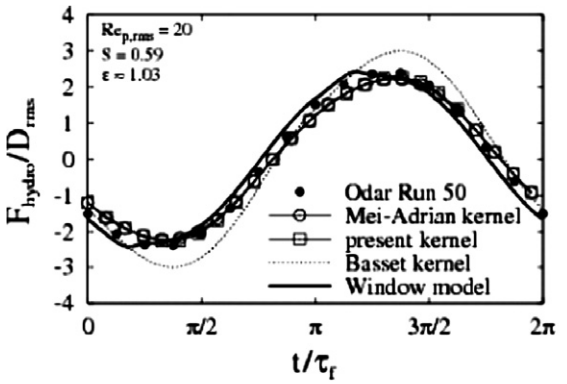

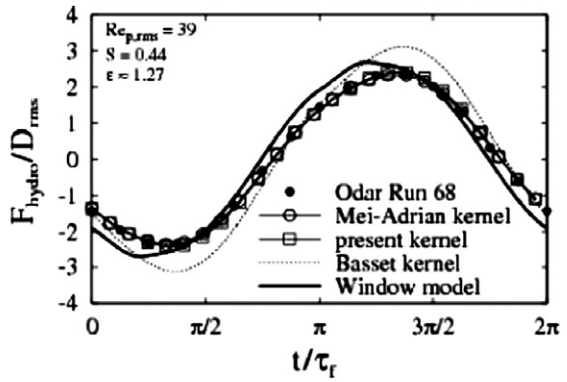

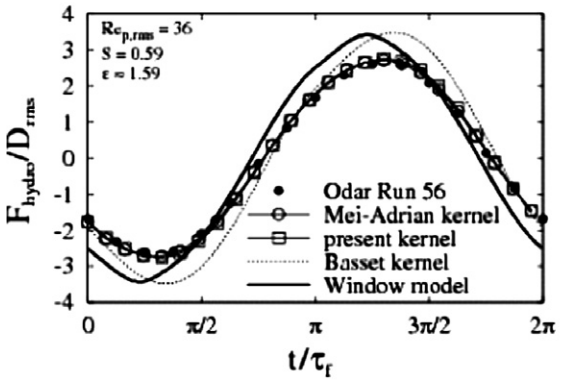

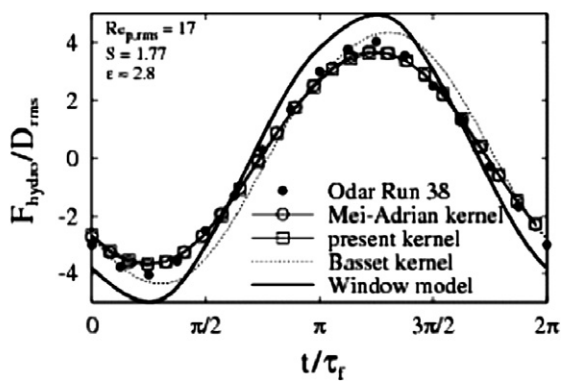

References

Armenio, V., Fiorotto, V., 2001. The importance of the forces acting on particles in turbulent flows. Phys. Fluids 13, 2437–2440.

Auton, T.R., Hunt, J.C.R., Prud'Homme, M., 1988. The force exerted on a body in inviscid unsteady non-uniform rotational flow. J. Fluid Mech. 197, 241–257.

Bataille, J., Lance, M., Marie, J.L., 1991. Some aspects of the modeling of bubbly flows. In: Hewitt, G.F., Mayinger, F., Riznic, J.R. (Eds.), Phase-Interface Phenomena in Multiphase Flow. Hemisphere Publishing Corporation.

Chang, E.J., Maxey, M.R., 1994. Unsteady flow about a sphere at low to moderate Reynolds number, Part I oscillatory motion. J. Fluid Mech. 277, 347–379.

Crowe, C.T., Sommerfeld, M., Tsuji, Y., 1998. Multiphase Flows with Droplets and Particles. CRC Press, LLC, Boca Raton, FL.

Dorgan, A.J., Loth, E., 2004. Simulation of particles released near the wall in a turbulent boundary layer. Int. J. Multiphase Flow 30, 649–673.

Druzhinin, O.A., Elghobashi, S., 1998. Direct numerical simulations of bubble-laden turbulent flows using the two-fluid formulation. Phys. Fluids 10, 685–697.

Kim, I., Elghobashi, S., Sirignana, W.B., 1998. On the equation for spherical-particle motion: effect of Reynolds and acceleration numbers. J. Fluid Mech. 367, 221–253.

Lawrence, C.J., Mei, R., 1995. Long-time behaviour of the drag on a body in impulsive motion. J. Fluid Mech. 283, 307–327.

Loth, E., 2000. Numerical approaches for motion of dispersed particles, bubbles, and droplets. Progr. Energy Combust. Sci. 26, 161–223.

Lovalenti, P.M., Brady, J.F., 1993. The force on a sphere in a uniform flow with small-amplitude oscillations at finite Reynolds number. J. Fluid Mech. 256, 607–614.

Lovalenti, P.M., Brady, J.F., 1995. The temporal behavior of the hydrodynamic force on a body in response to an abrupt change in velocity at small but finite Reynolds numbers. J. Fluid Mech. 293, 35–46.

Maxey, M.R., Riley, J.J., 1983. Equation of motion for a small rigid sphere in a non-uniform flow. Phys. Fluids 26, 883–889.

Mei, R., 1994. Flow due to an oscillating sphere and an expression for unsteady drag on the sphere and finite Reynolds number. J. Fluid Mech. 270, 133–174.

Mei, R., Adrian, R.J., 1992. Flow past a sphere with an oscillation in the free-stream velocity and unsteady drag at finite Reynolds number. J. Fluid Mech. 237, 323–341.

Mei, R., Klausner, J.F., 1992. Unsteady force on a spherical bubble with finite Reynolds number with small fluctuations in the free-stream velocity. Phys. Fluids A: Fluid Dyn. 4, 63–70.

Mei, R., Lawrence, C.J., Adrian, R.J., 1991. Unsteady drag on a sphere at finite Reynolds number with small fluctuations in the free-stream velocity. J. Fluid Mech. 233, 613–631.

Moorman, R.W., 1955. Motion of a spherical particle in the accelerated portion of free-fall. Doctor of Philosophy Dissertation, University of Iowa.

Mordant, N., Pinton, J-F., 2000. Velocity measurement of a settling sphere. Eur. Phys. J. B 18, 343–353.

Odar, F., 1962. Forces acting on a sphere accelerating in a viscous fluid. Doctor of Philosophy Dissertation, Northwestern University.

White, F.M., 1991. Viscous Fluid Flow. McGraw-Hill, New York.